Comparison of the adsorption of linear and cyclic antimicrobial peptides onto cellulosic compounds-reinforced poly(vinyl alcohol) films using QCM-D

Marta A. Teixeira [a], N. Sanjeeva Murthy [b], Diana P. Ferreira [a], Helena P. Felgueiras [a,*]

[a] *Centre for Textile Science and Technology (2C2T), Department of Textile Engineering, University of Minho, Campus of Azurém, Guimarães 4800-058, Portugal*
[b] *New Jersey Center for Biomaterials, Rutgers - The State University of New Jersey, 145 Bevier Road, Piscataway, NJ 08854, USA*

G R A P H I C A L   A B S T R A C T

A R T I C L E   I N F O

A B S T R A C T

Understanding peptide adsorption kinetics onto biomaterial surfaces is crucial for developing wound treatments. This study aims to explore the influence of cellulose acetate (CA) and cellulose nanocrystals (CNC) on peptide adsorption via quartz crystal microbalance with dissipation monitoring (QCM-D), using a cyclic peptide, Tiger 17, and a linear, Pexiganan. PVA was reinforced with 10 and 20% w/v of CA and CNC, spin-coated onto QCM-D sensors, and crosslinked with glutaraldehyde. Films containing higher percentages of cellulosic compounds promoted the highest peptide adsorption, with CNC-containing films being the most effective. While C80/20 PVA/CNC films achieved adsorption masses of ≈199 and ≈150 ng/cm² for Tiger 17 and Pexiganan, respectively, the C80/20 PVA/CA films attained ≈168 and ≈122 ng/cm². The peptides' structure also influenced adsorption, with Tiger 17 reaching greater frequency drops (ΔF) than Pexiganan. Sequential adsorption studies corroborated these findings. Even though the tendency was for PVA/CNC to promote the highest peptide binding, it was the PVA/CA films that reached the greatest peptide loading amount with the sequence Pexiganan + Tiger 17. Data are encouraging for developing new wound therapies reinforced with cellulosic compounds and modified with Tiger 17 and Pexiganan.

1. Introduction

Chronic wounds (CW) affect more than 40 million patients globally. In Europe alone, 4 million patients suffer from chronic wounds every year. CW results in considerable effects on one's life and substantial medical costs. In many cases, lack of suitable treatment formulations may lead to serious infections [1]. Infection is recognized as a hindering factor in the CW healing cascade, with the administration of systemic antibiotic therapies being the standard treatment tool in wound management. However, use of antibiotics has resulted in ever-increasing development of microbial resistance, along with unavoidable adverse side effects to other cell tissues and organs and ineffective delivery because of damaged blood vessels [2]. Topical applications to the wound site, such as wound dressings, can improve drug efficiency via an effective delivery, while reducing dosage and avoiding the previously mentioned issues [3]. Topical formulations derived from functionalizing polymeric structures with drugs, nanoparticles, natural extracts, and/or other biomolecules, like growth factors, hormones, enzymes, and peptides have contributed greatly to the effectiveness of the wound healing process [4].

Interest in peptides with regenerative and antimicrobial capacities has increased in the last years considering the growing investment in developing immunomodulatory therapies and infection management surfaces [5]. Tiger 17 was firstly reported by Tang *et al.* in 2014 [6]. Tiger 17 is a cyclic peptide of 11 amino acid residues derived from tigerinin precursors isolated from skin secretions of the *Fejervarya cancrivora* frog [7]. In this study, Tiger 17 was shown to play a significant role in the inflammatory stage of diabetic foot ulcers. It was seen to recruit macrophages to the wound bed as well as promote the re-epithelialization and granulation tissue formation by promoting proliferation and migration of keratinocytes and fibroblasts. In addition, this peptide also showed to promote the release of mitogen-activated protein kinases, interleukin 6, and transforming growth factor β1 in murine macrophages in the remodeling phase [6]. More recently, we uncovered the effectiveness of Tiger 17 against *Pseudomonas aeruginosa and Staphylococcus aureus* bacteria and established its excellent capacity for promoting keratinocytes and fibroblasts proliferation and to accelerate blood clotting above other peptides (i.e., Pexiganan) and materials (i.e., glass [8]). Antimicrobial peptides (AMPs) are very promising in infection control due to their ability in mitigating microbial propagation, reducing antibiotic resistance, and by acting against a broad variety of microorganisms decreasing the need for secondary drugs [9]. Most AMPs are molecules composed of 5–100 amino acids [6]. Despite their different amino acid sequences, they share a cationic nature due to the prevalence of lysine, arginine, and histidine that makes them resistant against bacteria, fungi, unicellular protozoa, and viruses. Moreover, AMPs display an amphiphilic structure which allow these molecules to bind to lipid components (hydrophobic regions) and phospholipid groups (hydrophilic regions) [10]. Pexiganan, also known as MSI-78, is one of the most well studied AMPs, being composed of a synthetic 22 amino acid residue, analogue of magainin, isolated from the skin of the African clawed frog *Xenopus laevis* [11]. This peptide possesses a α-helical structures and exhibits a broad spectrum of antimicrobial activity against both Gram-positive and Gram-negative bacteria [12]. It acts directly on the anionic phospholipids of the bacterial cell membrane and not on membrane receptors, turning the development of resistance theoretically less likely [13]. Pexiganan has been incorporated in topical creams reaching a phase III clinical trial for the treatment of mild infections in diabetic foot ulcers; however, it has not surpassed the efficacy of conventional antibiotics, requiring additional clinical studies, including assessment of its effectiveness in treating surgical wounds, burns, and decubitus ulcers [7]. Thus, a molecular-level understanding of protein/peptide adsorption and cell response on polymeric surfaces will be helpful in developing novel and efficient scaffolding systems (i.e., drug delivery platforms, dressing systems, etc.) [14].

Quartz crystal microbalance with dissipation monitoring (QCM-D) is a technique used to quantify the amount of peptide bound to the surface of biomaterials and to examine events of molecule-surface interaction in real-time [15]. In QCM-D, the deposition of a substance on the surface of a sensor decreases its resonating frequency and, depending on the viscoelastic properties of the tested molecules, changes the energy dissipation [16]. With 10 and 5 MHz resonant frequency, a frequency change of 1 Hz corresponds to a change in mass of 4.4 and 17.7 ng, respectively. Thus, a QCM-D system is about 100 times more sensitive than a typical precise analytical balance, enabling observation of mass changes at a nanogram level and giving the ability to distinguish even atomic monolayers [17]. Dissipation refers to the oscillation energy that is lost when a molecule is adsorbed onto a substrate, and depends on the rigidity of the deposited layer, with dissipative losses are higher with soft layers than with rigid layers [18].

To study the affinity and the adsorption kinetics of peptides to a polymer, the substrate is generally prepared by spin coating the polymer from a solution onto the QCM-D sensor. Spin-coating technique has been widely used to modify the surface of a QCM-D sensor due to its simplicity, availability, quick coating/film production, and cost-effectiveness [19]. The centrifugal forces generated by spinning, spread the solution to form a thin, uniform film [20]. Synthetic polymers are easily processed via this approach. Polymers can endow a substrate of choice with tunable mechanical and chemical properties for many biomedical purposes, including mapping protein and peptide adsorption kinetics via QCM-D [21]. Poly(vinyl alcohol) (PVA), for example, is known for its high hydrophilic, non-toxic and biocompatible nature. Its physicochemical properties, such as high capacity for deformation and flexibility, low rigidity, and slow degradation kinetics are highly suited for wound dressings. However, many synthetic polymers, including PVA, lack protein affinity leading to poor cell attachment [22]. To overcome this limitation, PVA can be blended with bio-based polymers derived from natural resources, such as the acetate ester of cellulose (CA) and cellulose nanocrystals (CNC). Different ratios of PVA/CA and PVA/CNC were selected: 100/0, 90/10 and 80/20% w/v with the objective of integrating the cytocompatibility and the low immunogenicity of CA and the large surface area of CNC with the well-established flexibility, mechanical resilience, and biodegradability of PVA, and through that enhance peptide adsorption. Overall, the aim of this study was to assess the adsorption affinity of the cyclic Tiger 17 and the linear Pexiganan peptides onto polymeric composites containing cellulosic compounds. Their mutual influence by sequential adsorption experiments was also analyzed. Peptides adsorption was monitored in real-time using the QCM-D technique. To the best of the authors' knowledge, the affinity between structurally different peptides and cellulosic reinforcements in spin-coated substrates subjected to a glutaraldehyde vapor crosslinking directly over the sensor surface has yet to be explored via QCM-D.

2. Materials and methods

2.1. Materials

Polyvinyl alcohol (PVA, Mw 78,000 g/mol and 88% hydrolysis) was obtained from Polysciences, Inc. (USA), cellulose acetate (CA, Mw 30.000 g/mol and 39.8 wt% acetyl content) from Sigma-Aldrich (USA), and cellulose nanocrystals (CNC, diameters of $\approx$ 75 nm and polydispersity index of 0.181) from CelluForce (Canada). Acetic acid (glacial, $\geq$ 99%), glutaraldehyde (GA, 25% aqueous solution, $\geq$ 98%) and 11-amino-1-undecanethiol hydrochloride (AUT, $\geq$ 98%) were obtained from Sigma-Aldrich. The reagents for cleaning the sensors, namely dimethyl sulfoxide (DMSO, $\geq$ 99.5%), Milli-Q ultrapure water, ammonium hydroxide (30%), and hydrogen peroxide (30%) were also obtained from Sigma-Aldrich. Gold-coated QCM-D sensors (QSX301, 14 mm diameter and AT-cut, with nominal resonant frequency of

4.95 MHz) were purchased from Biolin Scientific (Sweden). Tiger 17 (c [WCKPKPKPRCH-NH2], 1376.9 Da, purity > 95%) and cysteine-modified Pexiganan (cys-GIGKFLKKAKKFGKAFVKILKK-NH$_2$, 2581.1 Da, purity > 95%) peptides were provided by Isca Biochemicals (UK). All reagents were used without further purification.

2.2. QCM-D sensor preparation

Gold QCM-D sensors were cleaned with DMSO for 1 h in an ultra-sonic bath, followed by soaking in a 5:1:1 v/v/v mixture of Milli-Q ultrapure water, ammonia (25% w/w), and hydrogen peroxide (30% w/w) at 80 °C for 15 min. The sensors were then rinsed with Milli-Q ultrapure water and dried with filtered nitrogen, and finally irradiated for 20 min with UV/ozone (UVO-Cleaner model #42, Jelight, USA). To increase the adhesion of the polymeric layer to the sensors' surface during coating, droplets of an ethanolic solution containing 1 mM of AUT were placed over the sensors and left overnight at 4 °C. Afterwards, the excess AUT was removed by rinsing with Milli-Q ultrapure water before spin coating.

2.3. QCM-D sensor coating

Sensors were spin-coated with 2% (w/v) solutions of PVA/CA and PVA/CNC at three ratios: 100/0 (or 100% PVA), 90/10 and 80/20% (w/v), covering the entire surface (without impairing the sensors sensibility during QCM-D measurements). The PVA/CA solutions were prepared in 75/25% (v/v) acetic acid/distilled water (dH$_2$O) at 70 °C for 3 h, while the PVA/CNC were prepared in dH$_2$O for 4 h at 70 °C. Before spin-coating, the viscosities of the polymeric solutions were determined at room temperature (RT) using a Viscometer (Brookfield DV – II+ Pro with a 21 spindle). Spin-coating was conducted inside a glovebox flushed with filtered, dry air, using a Headway Research EC101DT-R485 Photo-Resist spin coater (30 s at a spin speed of 3000 rpm). 150 μL of polymer solution were dispensed on the surface, ensuring complete coverage. The spin-coated sensors were dried overnight at 60 °C. The stability of the PVA film on the sensors was achieved via crosslinking process with GA vapor at 80 °C for 6 h. Each sensor was subjected to 0.750 mL of GA vapor inside a vacuum-sealed desiccator. Before QCM-D experiment, any excess GA was removed from the surfaces by drying the sensors overnight at 80 °C. Uncrosslinked sensors were labelled as 100/0, 90/10 and 80/20, and the crosslinked sensors as C100/0, C90/10, and C80/20.

2.4. Surface characterization

2.4.1. Scanning electron microscopy (SEM)
SEM micrographs of the spin-coated sensors before and after crosslinking were obtained using NOVA 200 Nano SEM (FEI Company) with an accelerating voltage of 10 kV, without a gold ultra-thin coating being applied. Images at 16,000x magnification were taken to analyze the surface morphology.

2.4.2. Fourier-transform infrared spectroscopy in attenuated total reflectance mode (ATR-FTIR)
The chemical structure of the spin-coated polymeric films, the effectiveness of the crosslinking process, and the presence of residual GA were assessed via ATR-FTIR spectra collected using a NicoletTM iS10 FTIR Spectrometer (Thermo Fisher Scientific, USA), equipped with a diamond crystal. Data were collected at a spectral resolution of 8 cm^{-1}, by performing 45 scans from 4000 to 550 cm^{-1}.

2.4.3. Contact angle measurements
Water contact angle measurements were made using the OCA 20 DataPhysics apparatus (Filderstadt, Germany), equipped with a video-based drop shape analyzer OCA15 and associated software (version 1.2) following the ASTM-D7334–08 protocols. Droplets of 5 μL of dH$_2$O and a dosage rate of 1 μL/s were used to evaluate the films wettability via the sessile drop measuring method at 23 °C and a humidity of ≈ 50%. Angles were recorded immediately after the drop contacted the surface. Each spin-coated sensor was analyzed for its wettability on at least three randomly selected spots and the data were averaged.

2.5. Peptide adsorption studies

2.5.1. QCM-D analyses
A QCM-D system (Q-Sense E4 instrument, Biolin Scientific, Sweden) was used to monitor the frequency (ΔF) and dissipation (ΔD) shifts associated with peptide adsorption onto the PVA/CA and PVA/CNC spin-coated sensors, overtime. Coating thickness was also determined.

2.5.1.1. Single-peptide adsorption studies. An initial baseline was obtained with Milli-Q ultrapure water for 20 min. Afterwards, Tiger 17 and Pexiganan were individually introduced into a QCM-D module. Peptide solutions were prepared in Milli-Q ultrapure water according to their minimum inhibitory concentrations (MICs): Tiger 17, because of its antimicrobial limitations, was prepared at 40 μg/mL (twice the concentration required for inducing regenerative effects on CW, as determined by Tang *et al.* [6]); Pexiganan was prepared at 128 ug/mL (2×MIC) [7]. The flow was maintained until equilibrium (peptide saturation) was reached and then, it was stopped. In the end, a rinsing procedure was performed to remove the weakly bound peptides by flowing Milli-Q ultrapure water for 10 min. All QCM-D experiments, including baseline, rinsing and peptide adsorption, were performed at a constant flow rate of 5 μL/min and at RT.

2.5.1.2. Sequential peptide adsorption studies. Sensors coated with PVA/CA and PVA/CNC polymeric films were exposed sequentially to the two peptides: (1) Tiger 17 + Pexiganan, and (2) Pexiganan + Tiger 17. Sensors without any coating were used as control. Peptide solutions were prepared as described in the previous section. The adsorption of the first peptide was followed until saturation, and then the second peptide was flown into the module until a new adlayer reached equilibrium. Between peptide injections and at the end of the second peptide introduction, Milli-Q ultrapure water was introduced for 10 min to perform a rinsing procedure to remove poorly bound molecules.

2.5.1.3. QCM-D data analysis. Since the shifts in dissipation in response to peptide adsorption were less than 1×10^{-6} Hz^{-1} per 20 Hz drop in frequency, the Sauerbrey equation, Eq. (1), was used to determine the absorbed mass (expressed in ng/cm^2) [16]:

$$\Delta m = -\frac{\Delta F(Hz)}{n} * C \tag{1}$$

where Δm is the adsorbed mass, ΔF is the shift in frequency, n is the overtone number, and C is the mass sensitivity of a sensor with a fundamental frequency of 4.95 MHz (17.7 ng/cm^2.Hz). Data from the 3rd to the 11th overtones were collected. Peptide adsorption data was analyzed using QTools software (Biolin Scientific, Sweden).

AUT, PVA/CA and PVA/CNC layers thicknesses on top of the sensors were also determined.

To determine the AUT layers and PVA/CA and PVA/CNC films thicknesses, a clean QCM-D sensor was mounted in the QCM-D module and a stable baseline data was recorded and saved in individual files. Then, the AUT layer and the different PVA/CA and PVA/CNC films were deposited on these clean QCM-D sensors. Each one of these sensors was remounted and a stable baseline data was recorded again and saved in another file. The two collected frequency data files for each layer/film (those from the clean, uncoated QCM-D sensor and that of the same sensor but after coating) were stitched using the "Stitch Data Files" function provided in QTools software and the layers thicknesses were determined by dividing Δm, obtained from the Sauerbrey equation, using AUT and polymeric density of 0.9 g/cm^3 and 1.2 g/cm^3, respectively.

2.6. Statistical analysis

All experiments were conducted in triplicate. Numerical data were reported as mean ± standard deviation (S.D.). Statistical significance was determined by One-Way ANOVA via Kruskal-Walli's test using GraphPad Prism 9.0 software. Multiple comparisons were obtained via Dunn's test. Significance was defined as having $p<0.05$.

3. Results

3.1. Characterization of solutions and polymeric films' surface

100/0, 90/10 and 80/20% w/v PVA/CA and PVA/CNC spin-coated films were successfully deposited onto the QCM-D sensors. The viscosity of solutions, spin speed, spin-time, solvent evaporation rate and surface wettability are factors which define film' thickness produced by a spin-coater [20]. Here, CA-containing films shown thicker than CNC-containing films (Table 1). As spin speed and spin-time of production of films were the same for all films produced, these differences in thickness appear to be related to the viscosity values of the solutions. Solutions' viscosity increased with CA incorporation, in contrast with CNC-containing solutions.

To ensure the stability of the films in aqueous media, the spin-coated films were subject to a crosslinking process with GA vapor. The effectiveness of the crosslinking was corroborated by achieving a stable baseline during Milli-Q ultrapure water introduction. During these initial 20 min, no variation in frequency and dissipation were detected (Fig. 2 and Fig. 4). PVA-coated sensors exposed to vapors generated by 0.750 mL of GA inside a vacuum-sealed desiccator at 80 °C, for 6 h were deemed effective conditions to attain the stability needed. After crosslinking, films' thickness increased by ≈ 15, 106 and 171% for C100/0, C90/10, and C80/20 PVA/CA, respectively; the corresponding values for PVA/CNC spin-coated films, were ≈ 56, 41 and 76% (Table 1).

Since peptides' adsorption kinetics is influenced by the topography, morphology, chemical composition and wettability of the substrates, SEM, ATR-FTIR and contact angle evaluations were made on the crosslinked spin-coated films.

Figure S1 shows the uncrosslinked and crosslinked spin-coated 80/20% w/v PVA/CA surface on the QCM-D sensors (example used to represent the results obtained on all films produced). However, SEM micrographs were inconclusive since no morphology differences could be highlighted. Techniques such as ATR-FTIR and contact angle measurements were used to confirm the presence of these films on the QCM-D sensors and better uncover their properties. In this way, the effectiveness of blending of PVA with CA/CNC and the crosslinking processes were verified by ATR-FTIR (Fig. 1). The uncrosslinked films showed poorly defined spectra (with the exception of the thicker 80/20 spin-coated PVA/CA film) due to the smaller thickness of the film. It may be related with the depth readability of the equipment which ranges between 0.7 and 2.0 μm, with the spectra showing the contributions from the Au coating on the crystal.

All spectra showed PVA characteristic bands (highlighted on the PVA powder spectrum in Figure S2): -O–H stretching vibration (at around ≈

3346 cm^{-1}), the C–H stretching of the alkyl groups (≈ 2941 and 2921 cm^{-1}), the C═O stretching bond of acetate groups (≈ 1738 cm^{-1}), the C–H$_2$ bending vibrations (≈ 1436 cm^{-1} and ≈ 1374 cm^{-1}), the C–C skeletal vibration (≈ 1248 cm^{-1}), the C–C and C–O groups stretching vibrations (≈ 1090 cm^{-1}), the rocking vibration of CH$_2$ (≈ 903 cm^{-1}), and the C–C stretching vibrations, and the O–H out-of-plane bending vibrations (≈ 856 cm^{-1}) [23,24]. Even though not all these characteristic peaks were seen in all spectra, many were evident even in those thinner, uncrosslinked films. For example, in the spectra of PVA/CA 100/0 and 90/10, peaks around 3356 cm^{-1} did not appear but peaks at 1374 and 1253 cm^{-1} are present (highlighted in the graph). The same is true for the PVA/CNC combination.

Regarding the presence of cellulosic compounds, CA was mainly noted on the 80/20 PVA/CA spectrum by the presence of well-defined CA characteristics peaks at 1739 (νC═O), 1253 (νC-O) and 1051 cm^{-1} (stretching of glycosidic units -C-O-C-) [25]. In Figure S2, this last characteristic peak is detected at 1033 cm^{-1}, with the shift being justified by the CA bonding to PVA. In CNC-containing films, no significant difference was found on the spectra to confirm its presence. This may be related to the reduced thicknesses of the uncrosslinked and crosslinked films. The effectiveness of the crosslinking process is shown by the occurrence of bands at 1154 cm^{-1} and 1196 cm^{-1} in the spectra of PVA/CA and PVA/CNC crosslinked films, respectively, due to the formation of acetal bonds -O-C-O between both polymeric formulations and the crosslinker, GA [26]. Despite the C═O stretching bond of acetate groups from PVA at ≈ 1739 cm^{-1}, its intensification and its slight shift on PVA/CA crosslinked films demonstrated the presence of GA. It was also confirmed by its characteristic C═O stretching of aldehyde groups (Fig. 1 (A)) [27]. On its turn, the emergence of the band at ≈ 1700 cm^{-1} on the crosslinked PVA/CNC films was only possible because of the films' thickness improvement resultant from the crosslinking, which confirmed its effectiveness. From the observations, it is possible to conclude that the uncrosslinked PVA and cellulosic compounds did not undergo chemical reaction but formed a physical blend, while in crosslinked spin-coated films new bond formation could be discerned by the occurrence of new peaks.

The wettability of crosslinked films was measured via sessile drop method by applying a droplet of dH$_2$O over the films' surface and measuring the contact angle formed between the surface, the droplet, and the surrounding atmosphere. All crosslinked spin-coated films displayed a hydrophilic character as shown by the contact angles < 90° (Table 1). As CA content increased in the polymeric films, the wettability of the surfaces reduced, while with the presence of higher CNC content on the films, the wettability increased.

3.2. Single-peptide physical adsorption studies

Adsorption measurements performed via QCM-D technique provided information about the affinity of peptides towards the tested substrates. In QCM-D, increased mass adsorptions on the sensors' surface results in negative relative frequency shifts, ΔF, and mass reduction to positive shifts, assuming that the adsorbed layer is rigid, as is the case with our samples [18]. The adsorption kinetics of Tiger 17 (40 μg/mL) and

Table 1

Polymeric solutions viscosities and thickness of AUT layer of spin-coated PVA/CA and PVA/CNC films before and after crosslinking, and wettability of the crosslinked films. Data is reported as mean ± S.D. (n = 3).

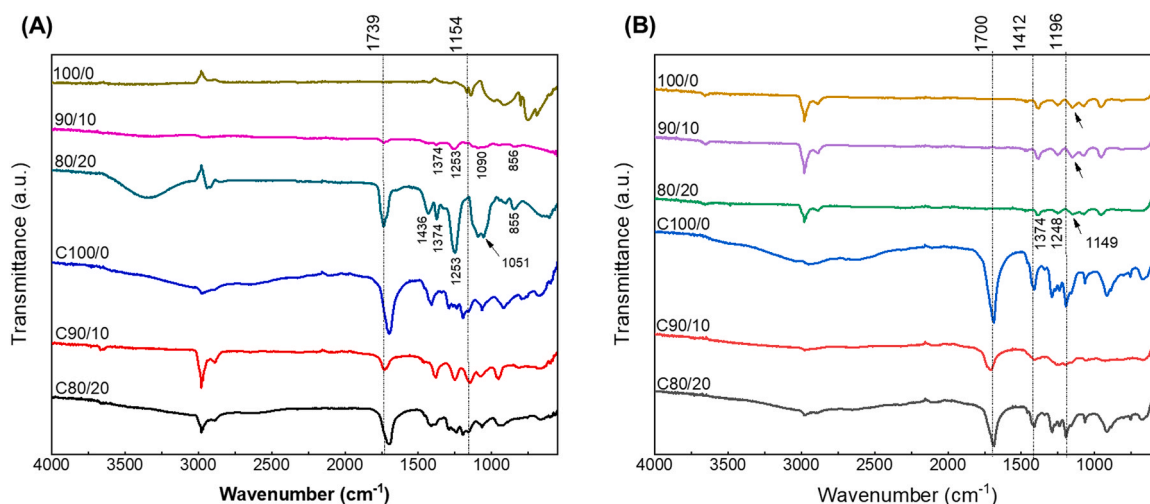| Polymer Ratio (% w/v)		Viscosity (cP)	Thickness (nm)			Contact angle (°)
			AUT Layer	Uncrosslinked Films	Crosslinked Films	
PVA/CA	100/0	20.9 ± 0.4	13.2 ± 4.6	147.8 ± 8.2	172.8 ± 6.9	72.8 ± 7.0
	90/10	32.1 ± 0.8	6.4 ± 2.7	152.3 ± 5.6	314.1 ± 1.9	73.6 ± 6.4
	80/20	32.0 ± 1.0	19.6 ± 5.2	162.5 ± 2.5	439.0 ± 7.0	75.4 ± 4.7
PVA/CNC	100/0	29.9 ± 1.3	3.1 ± 0.8	124.5 ± 4.5	194.0 ± 9.0	70.5 ± 2.9
	90/10	26.9 ± 0.8	5.3 ± 3.2	119.3 ± 8.2	167.4 ± 4.5	61.5 ± 5.0
	80/20	13.0 ± 0.2	4.1 ± 0.3	106.5 ± 8.5	186.1 ± 8.9	56.5 ± 3.2

Fig. 1. : ATR-FTIR spectra of the uncrosslinked and crosslinked (A) PVA/CA and (B) PVA/CNC spin-coated films. In (A), the arrow in the 80/20 combination highlights the C-O-C of glycosidic units present in cellulosic substrates, verifying the presence of CA in the film.

Pexiganan (128 µg/mL) peptides was monitored *in situ* on QCM-D sensors without any polymeric film (control sensors) and on sensors spin-coated with C100/0, C90/10 and C80/20 PVA/CA and PVA/CNC (Fig. 2).

Between the two peptides, Tiger 17 showed the highest ΔF drops in all substrates (Fig. 2), particularly on those containing cellulosic compounds, namely the CNC (Table S1). Rinsing with dH$_2$O showed negligible change in ΔF, indicating an irreversible attachment of the peptides

to all substrates. Changes in ΔF were translated into adsorbed peptide masses (ng/cm^2) and the respective times (min) for reaching saturation (Fig. 3 and Table S1).

Despite being at a lower concentration, Tiger 17 achieved the highest adsorption rates on the studied substrates and took the longest time to reach equilibrium (Fig. 3 and Table S1). The dissipation, ΔD, with Tiger 17 remained at zero, in most cases, with only a slight increase in C90/10 and C80/20 PVA/CNC. Pexiganan adsorption showed higher ΔD shortly
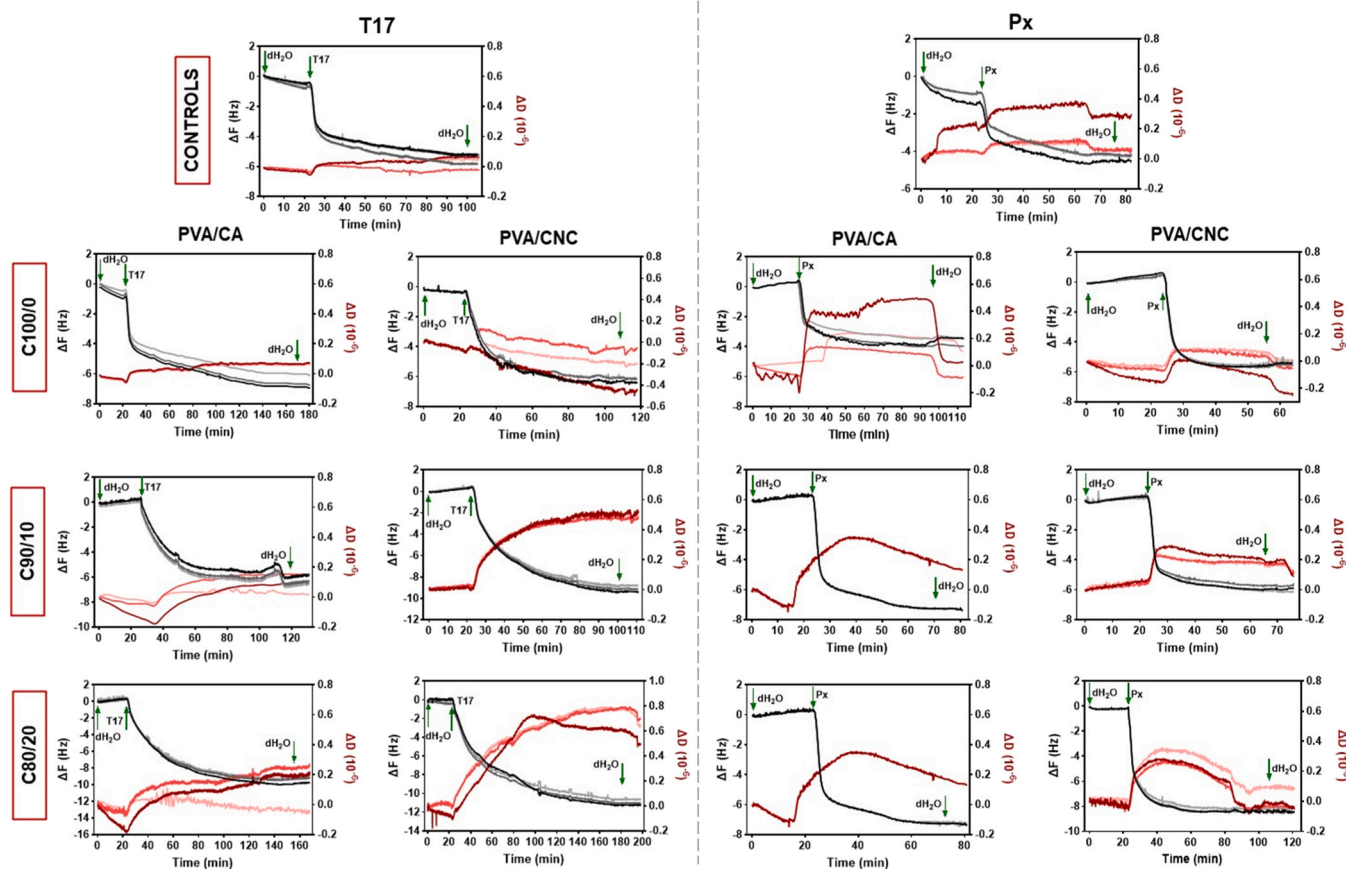

Fig. 2. : QCM-D frequency (ΔF) and dissipation (ΔD) plots of Tiger 17 (T17) and Pexiganan (Px) individual absorption profiles onto QCM-D sensors without any coating (control group) and spin-coated with C100/0, C90/0 and C80/20 PVA/CA and PVA/CNC. 3rd, 5th, and 7th overtones are shown, the higher the overtones the lighter the colors.

after the peptide's introduction and decreased slightly before reaching equilibrium (Fig. 2).

3.3. Sequential-peptide adsorption studies

The influence of one peptide on the adsorption profile of another was monitored on control and PVA/CA and PVA/CNC spin-coated sensors. Fig. 4 shows the changes in frequency and dissipation associated with the peptides' sequential adsorption onto the sensors. As expected, the adsorption profiles of Tiger 17 and Pexiganan introduced as first peptides in the sequences Tiger 17 + Pexiganan and Pexiganan + Tiger 17 were very similar to those reported in Fig. 2, both in ΔF and equilibrium times. As such, only the absorption of the second peptide onto an existing pre-adsorbed peptide layer is discussed here. With Tiger 17 as the second peptide, ΔF was larger than Pexiganan on all substrates; and ΔD decreased slightly. The only two exceptions were observed for the C100/0 and C80/20 PVA/CA films, where ΔD increased. In contrast, with Pexiganan as the second peptide in the sequence, ΔF decreased and ΔD increased. Changes in ΔF translated into adsorbed peptide masses (ng/cm^2) and the time required to reach equilibrium are shown in Fig. 5 and listed in Table S2.

4. Discussion

Immobilizing regenerative and antimicrobial peptides onto biomaterial surfaces can be a useful strategy to develop healing-inducing therapies for chronic wound care [8]. Towards this goal, two polymeric combinations containing cellulosic compounds, C100/0, C90/10 and C80/20 PVA/CA and PVA/CNC, were used to coat QCM-D sensors by spinning. Their influence on the adsorption kinetics of Tiger 17 (immunomodulatory peptide) and Pexiganan (antimicrobial peptide) presented to the surfaces in single or sequential modes was explored.

QCM-D sensors were modified with AUT to enhance the adhesion of the polymer films to the sensors' surface. AUT possesses thiol groups that bind to the gold coating of the sensors by strong metal-sulfur interactions (i.e., chemisorption), forming close-packed self-assembled monolayers, leaving the amine groups (-NH_2, the other end of n-alkanethiols) free [28]. Most of these amine groups are protonated under neutral conditions (pKa $\approx$ 7.5), thus establishing electrostatic interactions with the weakly negatively charged acetate groups of PVA ($\approx$ 12%) [29].

4.1. Characterization of solutions and polymeric films' surface

Presence of the AUT layers on top of the sensors was confirmed by thickness measurements (Table 1). PVA/CA and PVA/CNC films were deposited via spin-coating onto the AUT layer on the sensor surface. Films' thickness was determined after drying at 80 °C overnight. CA-containing films resulted in a thickness increase, in contrast with the PVA/CNC films (Table 1). This result may be related to the higher viscosity values of the CA-containing solutions due to a higher entanglement between the polymeric chains, in contrast with those CNC containing solutions that appear to interrupt the PVA chains entanglement. As the viscosity increases on CA-containing solutions more than CNC-containing solutions, the applied radial force easily loses the ability for the PVA/CA combination to spread across the surface and, hence, resulting in highest thicknesses [30]. To accomplish the structural stability of films during the peptide's adsorption test, GA, a well-established chemical crosslinker, was employed due to its effectiveness, low cost, and facile processing. Compared to its liquid-based strategies, the vapor phase crosslinking has been found to induce little cytotoxic effects [31]. After crosslinking, the average thicknesses of the PVA/CA and PVA/CNC films increased (Table 1); this could be due to the formation of acetal bonds between the aldehyde groups of GA and
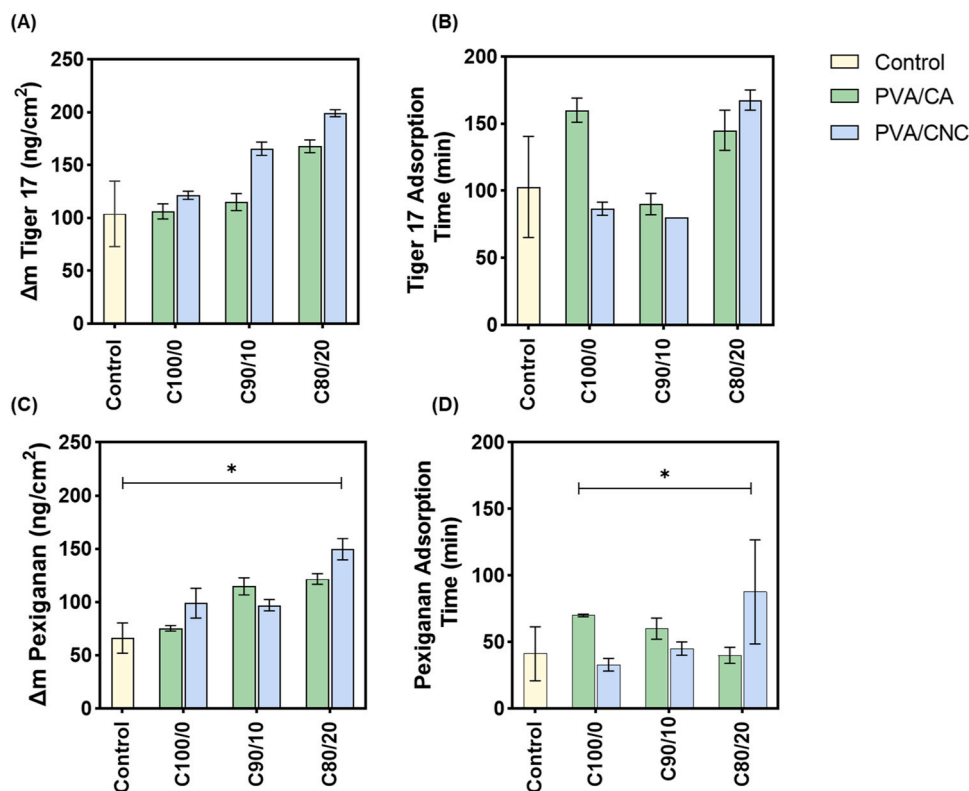

Fig. 3. (A, C) Tiger 17 and Pexiganan adsorbed mass on control sensors (without any polymeric film; yellow bars) and on C100/0, C90/10, and C80/20 PVA/CA (green bars) and PVA/CNC (blue bars) spin-coated sensors. (B, D) Time required for Tiger 17 and Pexiganan to reach surface saturation. Experiments were conducted at a flow rate of 5 μL/min. Statistical significance for (C) and (D) was determined via Kruskal-Walli's test applying multiple comparisons, being indicated by * (*p ≤ 0.05).
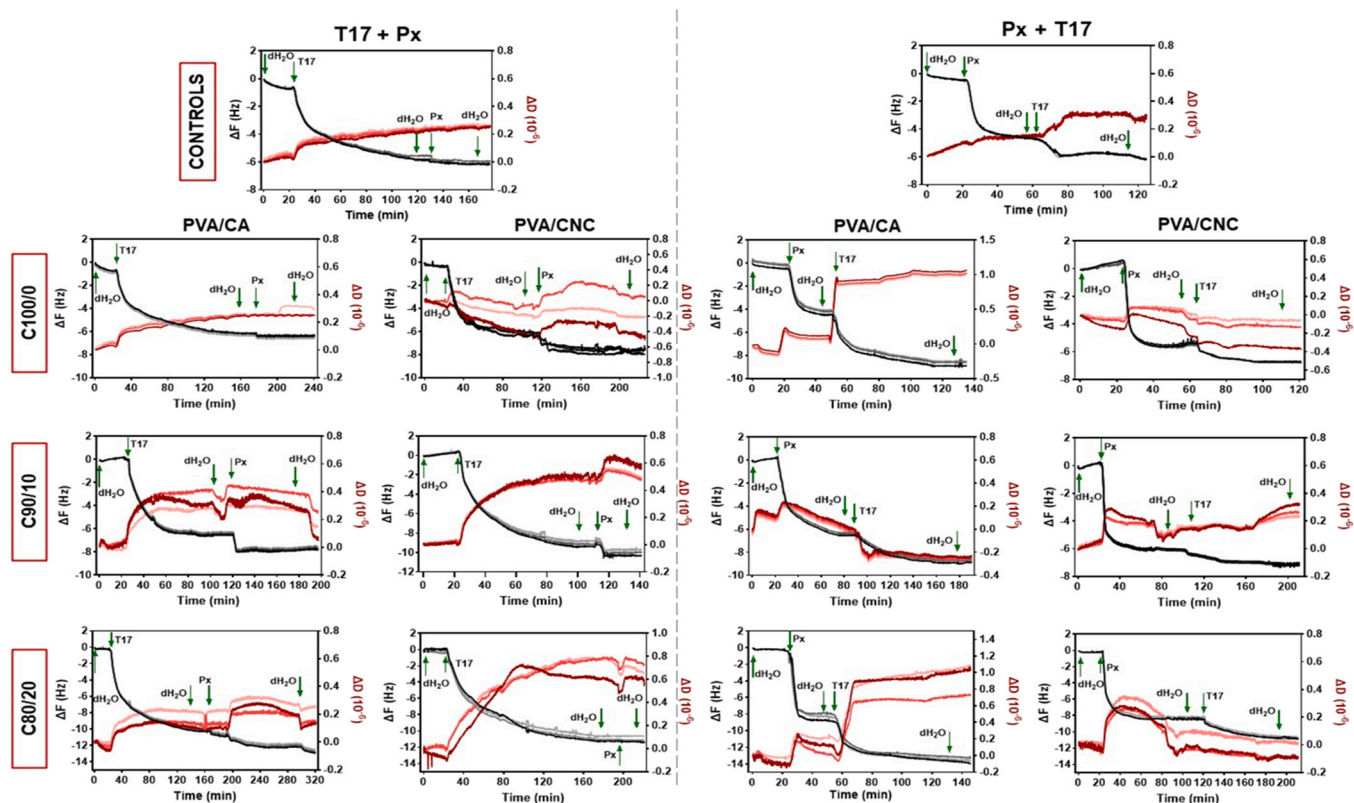
Fig. 4. : QCM-D frequency (Δf) and dissipation (ΔD) plots of Tiger 17 (T17) and Pexiganan (Px) sequential absorption profiles onto QCM-D sensors without any coating (control group) and spin-coated with C100/0, C90/0 and C80/20 PVA/CA and PVA/CNC. 3rd, 5th, and 7th overtones are represented, the higher the overtones the lighter the colors.

the hydroxyl groups of PVA, CA and CNC, as well as the swelling induced by the water molecules present in the GA solution [32].

The morphology, state of blending between polymers, crosslinking effectiveness, and wettability of the films was evaluated to understand their influence on the adsorption of the peptides. SEM micrographs of 80/20 and C80/20 films on top of the QCM-D sensors were inconclusive (Figure S1) in proving the presence of any film on the sensors' surface. In addition, no detectable differences in morphology were observed between all ratios of uncrosslinked and crosslinked films. Therefore, to demonstrate the presence of films on top of QCM-D sensors, ATR-FTIR and contact angle measurements were performed. The blending of both polymeric combinations and the effectiveness of the crosslinking process was confirmed by analyzing the ATR-FTIR spectra of the films on the QCM-D sensors (Fig. 1). Even though the ATR-FTIR spectra of the thin uncrosslinked films, with the exception of the thicker 80/20 PVA/CA film, showed the influence of the Au coating on the crystal, all spectra revealed characteristic PVA bands [33,34]. The presence of both cellulosic compounds was also seen in 90/10 and 80/20 spin-coated films. The emergence of a band at 1051 cm^{-1} (highlighted on Fig. 1), mainly in the 80/20 PVA/CA spectrum, indicated the stretching and deformation vibrations of glycosidic units -C-O-C- from the pyranose ring present in cellulosic substrates [25]. This band would be expected to be present in the spectra of CNC-containing films; however, it was not detected, most likely because of the small thickness of the films. Nevertheless, the presence of CNC could be confirmed by a reduction in the intensity of the band at ≈ 1700 cm^{-1} that is attributed to the residual acetate groups of the PVA matrix, and by a less accentuated band at 1240 cm^{-1} ascribed to the C-O stretching vibration of PVA (Fig. 1). The reduction of both bands is related with the shield effect caused by the presence of CNC; though, the reduction of the band at 1240 cm^{-1} has also been associated with the formation of hydrogen bonds between PVA

and CNC [35]. The effectiveness of the crosslinking process was also verified (Section 3.1).

The films' surface wettability, which affects protein/peptide adsorption, cell adhesion and, generally, the surface's anti-fouling capacity was also investigated. Several studies have shown the importance of material composition, roughness, and surface energy on this property [36]. All crosslinked spin-coated films displayed a hydrophilic character. These findings are in accordance with previous reports [37]. As the CA ratio increased in the blend, the contact angle also increased, since more hydrophobic acetyl groups ($\approx 40\%$) were present in the film [33]. This reduction in wettability emphasizes the formation of hydrogen bonds between PVA and CA, with fewer -OH groups remaining available. In the CNC-containing films, as the CNC ratio increased in the blend, the contact angle decreased, possibly due to an increase in the number of hydroxyl groups of CNC. Since highly hydrophilic and hydrophobic surfaces cannot promote cell adhesion and proliferation, maintaining wettability at moderate levels could be advantageous for wound healing applications (i.e., prevent excessive moisture absorption) [38].

4.2. Individual peptide adsorption studies

The adsorption of any molecule onto a biomaterial surface depends on the affinity and topography of that surface, contact duration, concentration, composition and dimensions of the molecules, ionic strength, presence of competing molecules in the solution, and the orientation the molecules adopt once bonded to the surface [38,39]. The peptide's structure has also been considered as another key factor influencing the interaction of peptides with biomaterials [40,41]. For instance, Choe *et al.* reported that the linear version of a Cu$_2$O-binding peptide does not bind to Cu$_2$O, whereas the cyclic version displays great affinity [41].
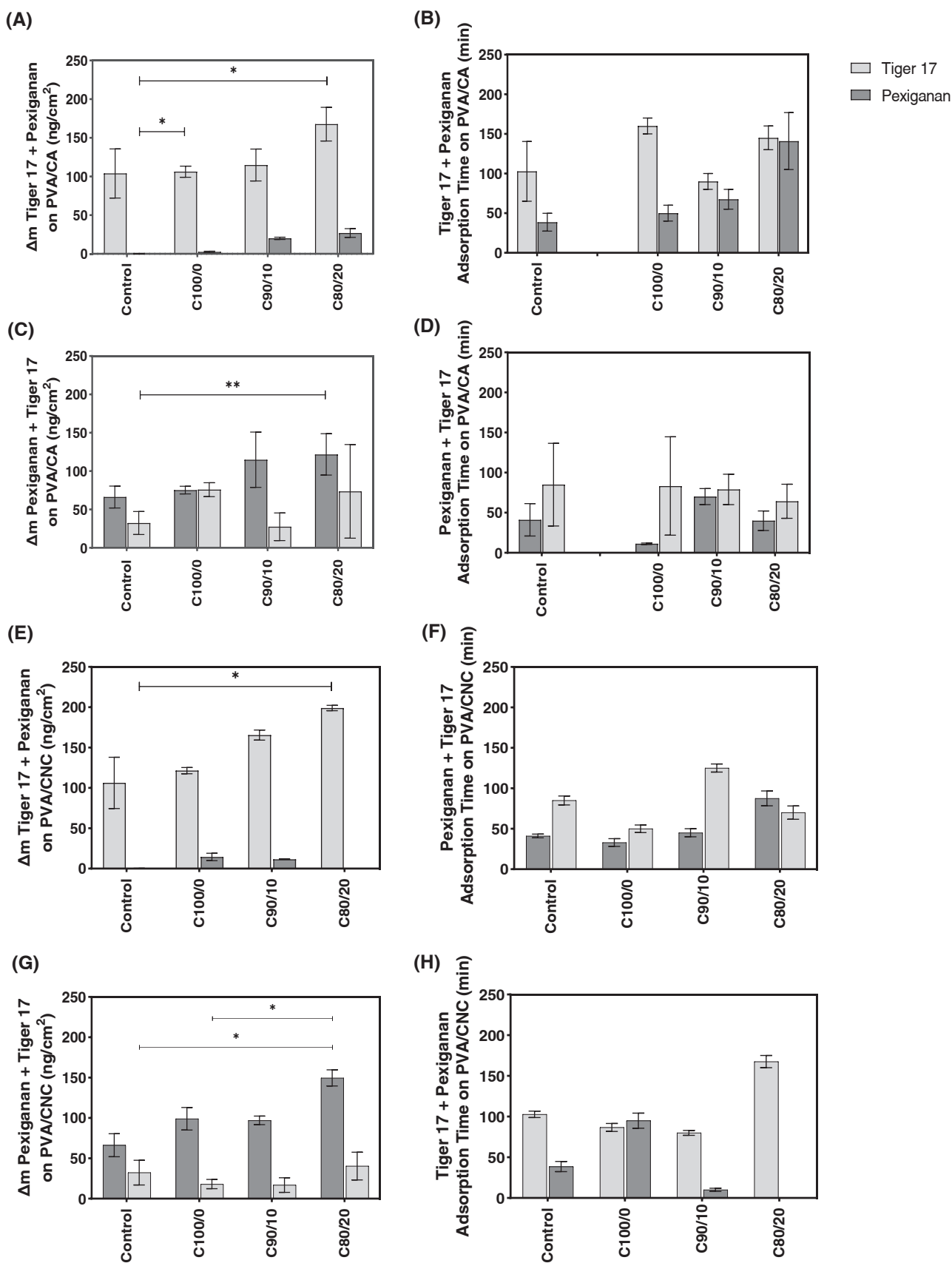
Fig. 5. (A, C) and (E, G): Tiger 17 and Pexiganan sequential absorption adsorbed mass (ng/cm^2) on control sensors and on C100/0, C90/10, and C80/20 PVA/CA and PVA/CNC spin-coated films, respectively. (B, D) and (F, H) Time required for Tiger 17 and Pexiganan sequential absorption to reach surface saturation. Experiments were conducted at a flow rate of 5 μL/min. Statistical significance was determined via Kruskal-Walli's test applying multiple comparisons, being indicated by * (*$p \leq 0.05$ and **$p \leq 0.01$).

Also, varying degrees of electrostatic interactions have been found between cyclic peptide STB1 (-CHKKPSKSC-) and SiO_2 and TiO_2 surfaces, while the binding behavior and the strength of interactions of its linear form (LSTB1) is similar towards both surfaces [40]. In this study, the adsorption of the small cyclic Tiger 17 peptide resulted in the highest drop in ΔF, on all tested substrates, and ΔD remained unchanged at zero, indicating that the Tiger 17 molecules adsorbed in the form of a rigid laterally homogeneous film [42]. This may be due to its cyclic structure and small chain dimensions. According to several studies, the cyclic structure may confer Tiger 17 with a rigid conformation, as consequence of the constraints exerted by the presence of the covalent C-C loop [8]. Its compact structure imposes restrictions on the peptide motion and the binding dynamics, contributing to a side-chain accessibility and orientation at the target surface, hence promoting a superior surface affinity [43]. Pexiganan, being a 22-amino acid linear peptide with large degree of conformational freedom, may promote multi-site binding [44]. In addition to their structural differences, the interaction of the peptides with the surfaces is also dependent on the chemical composition (e.g., charges) [10,45]. Peptide adsorption was greater on films with higher content in cellulosic compounds, namely on CNC-containing films (Figs. 3a and 3c). Between the peptides, Tiger 17 attained the highest adsorption rates (Figs. 3a and 3c). Cellulosic compounds might play a role in enhancing hydrophobic and electrostatic interactions between the surfaces and the peptides, and thus improving the adsorption of both peptides [46].

Hydrophobic interactions may play a larger role in PVA/CA films due to the inherent hydrophobicity of the CA acetate groups. Additionally, PVA chains contain acetate groups arising from the polymer incomplete hydrolysis. Hydrophobic interactions can occur between these acetate groups and the hydrophobic amino acids present on the peptides: three cyclic prolines distributed along the Tiger 17 chain and a tryptophan positioned at the N-terminus, and the leucine, isoleucine, and phenylalanine amino acids present in the Pexiganan chain [46]. Also, electrostatic interactions play an important role, especially when charged groups in the peptide chains move close to a solid surface with an opposite charge [47]. Generally, PVA-based material surfaces are negatively charged when in contact with physiological media. Positively charged amino acids like lysine, arginine and histidine can be found on Tiger 17, whereas lysine is widely present on the Pexiganan chain. Therefore, peptide adsorption may also be influenced by electrostatic attraction [48]. Enhanced adsorption on CNC-containing films may be a result of the larger number of strong and negatively charged groups, the sulfonates, which are generated during the CNC's extraction process [49]. CA and PVA also display negative acetate groups at physiological conditions; yet the sulfonate groups on the CNC surfaces are numerous, enhancing the ability of the PVA/CNC combination to establish electrostatic bonds with the peptides [50]. The small number of negative charges on the PVA chains may explain the reduced peptide adsorption on films composed only of PVA compared to those reinforced with cellulosic compounds. Regardless, peptide adsorption on PVA films was greater than on control gold surfaces that are negatively charged at high pH and weakly negatively charged at low pH, and thus being hydrophilic ($\approx 77°$) [51]. Hajiraissi *et al.* modified the structure of gold QCM-D sensors with different self-assembled alkanethiol monolayers (SAM) and noted that the negatively charged carboxylic acid-terminated SAM led to more effective adsorption rates than the hydrophobic, hydrophilic, and positively charged surfaces [52]. Thus, peptide adsorption onto the polymeric films may have originated from the strength and number of the negative charges available.

Peptides' concentration is another fact that influences the surface adsorption kinetics. Peptides at high concentrations and with high diffusion coefficients adsorb onto polymer surfaces rapidly due to their higher collision frequency [53]. This may explain why Pexiganan, introduced at a higher concentration (128 μg/mL) than Tiger 17 (40 μg/mL), reached equilibrium faster on all substrates. Also, considering its small and cyclic structure, a greater number of Tiger 17 molecules would be required to cover the surface, and thus the equilibrium time would be longer for Tiger 17 than for Pexiganan.

4.3. Sequential-peptide adsorption studies

The influence of PVA/CA and PVA/CNC spin-coated sensors, with varying cellulosic compounds contents, on the adsorption profile of one peptide after another was also assessed (Fig. 4). Here, the first peptide was introduced into the system and allowed to reach surface saturation, any poorly bound peptide molecules were removed from the surface by rinsing with distilled water, and subsequently a second peptide was added until equilibrium was again reached. As expected, the adsorption profiles of the first peptide in the sequences were very similar to those reported in the individual adsorption studies. Therefore, when the Tiger 17 was introduced as first peptide on the sequence Tiger 17 + Pexiganan, the decrease in ΔF was larger than that for Pexiganan for all substrates, as was reported in the individual adsorption results. The introduction of Tiger 17 as the first peptide significantly reduced the adsorption of Pexiganan as second peptide in relation to its individual rates (Fig. 4 and 5): $\approx 99\%$ on the control samples, between ≈ 78 and $\approx 97\%$ on PVA/CA films and between ≈ 85 and $\approx 100\%$ on PVA/CNC films. Similarly, Tiger 17 as the second peptide also experienced reductions of $\approx 69\%$ on the control, between ≈ 29 and $\approx 76\%$ on PVA/CA films and between ≈ 80 and $\approx 90\%$ on PVA/CNC films. With Tiger 17 as the first peptide that forms very rigid layer with a large number of molecules present on the substrates, the adsorption of Pexiganan, as second peptide, was hindered. Data also showed Pexiganan's inability to displace the pre-adsorbed Tiger 17 indicating this peptide's affinity to the surface, as well as its need for a larger surface area available for adsorption. In the sequence Pexiganan + Tiger 17, greater ΔF drops were seen for Tiger 17 as second peptide in comparison to the results with Pexiganan introduced as second peptide. This could be due to the soft layer that enabled Tiger 17 molecules to be absorbed in between the Pexiganan chains.

The highest rate of peptide absorption in the sequence studies were on films reinforced with cellulosic compounds (Fig. 4 and Fig. 5). Since both peptides are essential for a successful CW therapy, it is interesting to note Fig. 5 C that shows the Pexiganan + Tiger 17 sequence on PVA/CA films. Despite the low mass of the first peptide, the second peptide (Tiger 17) showed a greater mass compared to PVA/CNC films. In fact, the percentages obtained for Tiger 17 in relation to the total mass of peptides adsorbed on the sensors at the end of the sequential study were found between ≈ 19 and $\approx 50\%$ for PVA/CA films and between ≈ 15 and $\approx 21\%$ for PVA/CNC films. In contrast, Pexiganan, as a second peptide, reached a maximum of only $\approx 14\%$ on PVA/CA films and $\approx 11\%$ on PVA/CNC films. Once again, Tiger 17 was slower than Pexiganan in reaching equilibrium, even though the surface was already pre-loaded with peptide molecules. These analyses showed that larger amounts of peptide can be adsorbed onto polymeric surfaces by choosing the order in which the peptides are introduced, and by optimizing the materials' wettability and electrostatic features.

5. Conclusions

PVA reinforced with 10 and 20% w/v of CA and CNC were effectively deposited on QCM-D sensors. The presence of the polymers, namely PVA and CA, on the spin-coated films was confirmed by ATR-FTIR and contact angle measurements, confirming the blending. All films were hydrophilic, with small reductions in wettability observed at higher CA contents and small improvements with larger CNC amounts. Cross-linking by GA did not compromise the QCM-D measurements.

Peptides' adsorption was highest on cellulosic compounds-containing films, confirming the initial hypothesis. CNC-containing films contributed the most for the single adsorption of the peptides, highlighting its effectiveness in attracting Tiger 17 towards films with 20% w/v of CNC. Hydrophobic and electrostatic interactions between

surfaces and peptides were established more easily in the presence of cellulosic compounds, contributing to a greater and more effective adsorption.

The rigid cyclic structure and size of Tiger 17 contributed to superior drops in ΔF, taking longer to reach saturation. The affinity and rigidity of Tiger 17 was further demonstrated by the limited adsorption of Pexiganan in the sequence Tiger 17 + Pexiganan. In sequential-peptide adsorption studies, the highest peptide mass was detected on PVA/CA spin-coated sensors, namely in those with higher CA content. The inherent hydrophobicity associated with these films appeared to have influenced the distribution of the peptide molecules (also containing hydrophobic amino acids), promoting conformational rearrangements. The sequence Pexiganan + Tiger 17 promoted the highest adsorption rates, with Pexiganan flexible structure facilitating Tiger 17 adsorption in between the available spaces of its chains.

Data contributed to understanding the role of cellulosic compounds in the adsorption of structurally different peptides. More importantly, it was found that the presence of certain cellulosic compounds, as well as their quantity, are great effectors in peptide adsorption and to their optimal conformation arrangement, thus influencing peptide exposure along the biomaterial surfaces and, ultimately, their mechanisms of action fundamental for an effective wound treatment.

CRediT authorship contribution statement

Felgueiras Helena P.: Conceptualization, Funding acquisition, Methodology, Supervision, Writing – review & editing. **Ferreira Diana P.:** Funding acquisition, Supervision, Writing – review & editing. **Teixeira Marta A.:** Methodology, Validation, Writing – original draft, Writing – review & editing. **Murthy N. Sanjeeva:** Methodology, Supervision, Writing – review & editing.

Declaration of Competing Interest

The authors declare the following financial interests/personal relationships which may be considered as potential competing interests. Helena P. Felgueiras reports financial support was provided by Portuguese Foundation for Science and Technology. Marta A. Teixeira reports financial support was provided by Portuguese Foundation for Science and Technology. Diana P. Ferreira reports financial support was provided by Portuguese Foundation for Science and Technology.

Data availability

No data was used for the research described in the article.

Acknowledgments

Appendix A. Supporting information

Supplementary data associated with this article can be found in the online version at doi:10.1016/j.colsurfa.2024.133490.

References

[1] M. Falcone, B. De Angelis, F. Pea, A. Scalise, S. Stefani, R. Tasinato, O. Zanetti, L. Dalla Paola, Challenges in the management of chronic wound infections, J. Glob. Antimicrob. Resist 26 (2021) 140–147, https://doi.org/10.1016/j.jgar.2021.05.010.

[2] K. Wangoye, J. Mwesigye, M. Tungotyo, S. Twinomujuni Samba, Chronic wound isolates and their minimum inhibitory concentrations against third generation cephalosporins at a tertiary hospital in Uganda, Sci. Rep. 12 (2022) 1195, https://doi.org/10.1038/s41598-021-04722-6.

[3] S. Darmawati, A. Rohmani, L.H. Nurani, M.E. Prastiyanto, S.S. Dewi, N. Salsabila, E.S. Wahyuningtyas, F. Murdiya, I.M. Sikumbang, R.N. Rohmah, Y.A. Fatimah, A. Widiyanto, T. Ishijima, J. Sugama, T. Nakatani, N. Nasruddin, When plasma jet is effective for chronic wound bacteria inactivation, is it also effective for wound healing? Clin. Plasma Med. 14 (2019) 100085 https://doi.org/10.1016/j.cpme.2019.100085.

[4] S. Saghazadeh, C. Rinoldi, M. Schot, S.S. Kashaf, F. Sharifi, E. Jalilian, K. Nuutila, G. Giatsidis, P. Mostafalu, H. Derakhshandeh, K. Yue, W. Swieszkowski, A. Memic, A. Tamayol, A. Khademhosseini, Drug delivery systems and materials for wound healing applications, Adv. Drug Deliv. Rev. 127 (2018) 138–166, https://doi.org/10.1016/j.addr.2018.04.008.

[5] H.P. Felgueiras, An insight into biomolecules for the treatment of skin infectious diseases, Pharmaceutics 13 (2021) 1012, https://doi.org/10.3390/pharmaceutics13071012.

[6] J. Tang, H. Liu, C. Gao, L. Mu, S. Yang, M. Rong, Z. Zhang, J. Liu, Q. Ding, R. Lai, A small peptide with potential ability to promote wound healing, PLoS One 9 (2014), https://doi.org/10.1371/journal.pone.0092082.

[7] M.A. Teixeira, J.C. Antunes, C.L. Seabra, A. Fertuzinhos, S.D. Tohidi, S. Reis, M.T. P. Amorim, D.P. Ferreira, H.P. Felgueiras, Antibacterial and hemostatic capacities of cellulose nanocrystalline-reinforced poly(vinyl alcohol) electrospun mats doped with Tiger 17 and pexiganan peptides for prospective wound healing applications, Biomater. Adv. 137 (2022) 212830, https://doi.org/10.1016/j.bioadv.2022.212830.

[8] M.A. Teixeira, J.C. Antunes, C.L. Seabra, S.D. Tohidi, S. Reis, M.T.P. Amorim, H. P. Felgueiras, Tiger 17 and pexiganan as antimicrobial and hemostatic boosters of cellulose acetate-containing poly(vinyl alcohol) electrospun mats for potential wound care purposes, Int J. Biol. Macromol. 209 (2022) 1526–1541, https://doi.org/10.1016/j.ijbiomac.2022.04.130.

[9] H.P. Felgueiras, M.A. Teixeira, T.D. Tavares, M.T.P. Amorim, New method to produce poly(vinyl alcohol)/cellulose acetate films with improved antibacterial action, Mater. Today Proc. 31 (2020) S269–S272, https://doi.org/10.1016/j.matpr.2019.12.100.

[10] J. Talapko, T. Meštrović, M. Juzbašić, M. Tomas, S. Erić, L. Horvat Aleksijević, S. Bekić, D. Schwarz, S. Matić, M. Neuberg, I. Škrlec, Antimicrobial peptides—mechanisms of action, antimicrobial effects and clinical applications, Antibiotics 11 (2022) 1417, https://doi.org/10.3390/antibiotics11101417.

[11] M. Mahlapuu, C. Björn, J. Ekblom, Antimicrobial peptides as therapeutic agents: opportunities and challenges, Crit. Rev. Biotechnol. 40 (2020) 978–992, https://doi.org/10.1080/07388551.2020.1796576.

[12] J. Durão, N. Vale, S. Gomes, P. Gomes, C.C. Barrias, L. Gales, Nitric oxide release from antimicrobial peptide hydrogels for wound healing, Biomolecules 9 (2019), https://doi.org/10.3390/biom9010004.

[13] D. Gomes, R. Santos, R. S. Soares, S. Reis, S. Carvalho, P. Rego, M. C. Peleteiro, L. Tavares, M. Oliveira, Pexiganan in combination with nisin to control polymicrobial diabetic foot infections, Antibiotics 9 (2020), https://doi.org/10.3390/antibiotics9030128.

[14] U. Khan, K. Ryan, W.J. Blau, J.N. Coleman, The effect of solvent choice on the mechanical properties of carbon nanotube–polymer composites, Compos Sci. Technol. 67 (2007) 3158–3167, https://doi.org/10.1016/j.compscitech.2007.04.015.

[15] J. Naranda, M. Bračič, M. Vogrin, U. Maver, T. Trojner, Practical use of quartz crystal microbalance monitoring in cartilage tissue engineering, J. Funct. Biomater. 13 (2022) 159, https://doi.org/10.3390/jfb13040159.

[16] H.P. Felgueiras, S.D. Sommerfeld, N.S. Murthy, J. Kohn, V. Migonney, Poly(NaSS) functionalization modulates the conformation of fibronectin and collagen type i to enhance osteoblastic cell attachment onto Ti6Al4V, Langmuir 30 (2014) 9477–9483, https://doi.org/10.1021/la501862f.

[17] D. Migoń, T. Wasilewski, D. Suchy, Application of QCM in peptide and protein-based drug product development, Molecules 25 (2020) 3950, https://doi.org/10.3390/molecules25173950.

[18] D.I. Kushner, M.A. Hickner, Water sorption in electron-beam evaporated SiO2 on QCM crystals and its influence on polymer thin film hydration measurements, Langmuir 33 (2017) 5261–5268, https://doi.org/10.1021/acs.langmuir.7b00759.

[19] J. Moreira, A.C. Vale, N.M. Alves, Spin-coated freestanding films for biomedical applications, J. Mater. Chem. B 9 (2021) 3778–3799, https://doi.org/10.1039/D1TB00233C.

[20] N.-T. Nguyen, Fabrication technologies. in: Micromixers, Elsevier, 2012, pp. 113–161, https://doi.org/10.1016/B978-1-4377-3520-8.00004-8.

[21] H.P. Felgueiras, N.S. Murthy, S.D. Sommerfeld, M.M. Brás, V. Migonney, J. Kohn, Competitive adsorption of plasma proteins using a quartz crystal microbalance, ACS Appl. Mater. Interfaces 8 (2016) 13207–13217, https://doi.org/10.1021/acsami.5b12600.

[22] C.-Y. Huang, K.-H. Hu, Z.-H. Wei, Comparison of cell behavior on pva/pva-gelatin electrospun nanofibers with random and aligned configuration, Sci. Rep. 6 (2016) 37960, https://doi.org/10.1038/srep37960.

[23] A. López-Córdoba, S. Estevez-Areco, S. Goyanes, Potato starch-based biocomposites with enhanced thermal, mechanical and barrier properties comprising water-resistant electrospun poly (vinyl alcohol) fibers and yerba mate extract, Carbohydr. Polym. 215 (2019) 377–387, https://doi.org/10.1016/j.carbpol.2019.03.105.

[24] M.-C. Popescu, B.-I. Dogaru, M. Goanta, D. Timpu, Structural and morphological evaluation of CNC reinforced PVA/Starch biodegradable films, Int J. Biol. Macromol. 116 (2018) 385–393, https://doi.org/10.1016/j.ijbiomac.2018.05.036.

[25] P. Fei, L. Liao, B. Cheng, J. Song, Quantitative analysis of cellulose acetate with a high degree of substitution by FTIR and its application, Anal. Methods 9 (2017) 6194–6201, https://doi.org/10.1039/C7AY02165H.

[26] A.S. Rojas-Mercado, I.E. Moreno-Cortez, R. Lucio-Porto, L.L. Pavón, Encapsulation and immobilization of ficin extract in electrospun polymeric nanofibers, Int J. Biol. Macromol. 118 (2018) 2287–2295, https://doi.org/10.1016/j.ijbiomac.2018.07.113.

[27] M.C. Chang, J. Tanaka, FT-IR study for hydroxyapatite/collagen nanocomposite cross-linked by glutaraldehyde, Biomaterials 23 (2002) 4811–4818, https://doi.org/10.1016/S0142-9612(02)00232-6.

[28] P.R. Solanki, S.K. Arya, Y. Nishimura, M. Iwamoto, B.D. Malhotra, Cholesterol biosensor based on amino-undecanethiol self-assembled monolayer using surface plasmon resonance technique, Langmuir 23 (2007) 7398–7403, https://doi.org/10.1021/la700350x.

[29] K. Marcisz, M. Karbarz, Z. Stojek, Quartz crystal microbalance electrode modified with thermoresponsive crosslinked and non-crosslinked N-isopropylacrylamide polymers. Response to changes in temperature, J. Solid State Electrochem. 20 (2016) 3263–3270, https://doi.org/10.1007/s10008-016-3231-6.

[30] M.D. Tyona, A theoritical study on spin coating technique, Adv. Mater. Res. 2 (2013) 195–208, https://doi.org/10.12989/amr.2013.2.4.195.

[31] H. Tian, L. Yuan, J. Wang, H. Wu, H. Wang, A. Xiang, B. Ashok, A.V. Rajulu, Electrospinning of polyvinyl alcohol into crosslinked nanofibers: An approach to fabricate functional adsorbent for heavy metals, J. Hazard Mater. 378 (2019) 120751, https://doi.org/10.1016/j.jhazmat.2019.120751.

[32] H. Kamal, F.M. Abd-Elrahim, S. Lotfy, Characterization and some properties of cellulose acetate-co-polyethylene oxide blends prepared by the use of gamma irradiation, J. Radiat. Res Appl. Sci. 7 (2014) 146–153, https://doi.org/10.1016/j.jrras.2014.01.003.

[33] D.P. Ferreira, J. Cruz, R. Fangueiro, Surface modification of natural fibers in polymer composites. in: Green Composites for Automotive Applications, Elsevier, 2019, pp. 3–41, https://doi.org/10.1016/B978-0-08-102177-4.00001-X.

[34] M.R. Safaee-Ardakani, A. Hatamian-Zarmi, S.M. Sadat, Z.B. Mokhtari-Hosseini, B. Ebrahimi-Hosseinzadeh, J. Rashidiani, H. Kooshki, Electrospun Schizophyllan/polyvinyl alcohol blend nanofibrous scaffold as potential wound healing, Int J. Biol. Macromol. 127 (2019) 27–38, https://doi.org/10.1016/j.ijbiomac.2018.12.256.

[35] Z. Jahan, M.B.K. Niazi, Ø.W. Gregersen, Mechanical, thermal and swelling properties of cellulose nanocrystals/PVA nanocomposites membranes, J. Ind. Eng. Chem. 57 (2018) 113–124, https://doi.org/10.1016/j.jiec.2017.08.014.

[36] G.V. Kuznetsov, A.G. Islamova, E.G. Orlova, A.S. Ivashutenko, I.I. Shanenkov, I. Y. Zykov, D.V. Feoktistov, Influence of roughness on polar and dispersed components of surface free energy and wettability properties of copper and steel surfaces, Surf. Coat. Technol. 422 (2021) 127518, https://doi.org/10.1016/j.surfcoat.2021.127518.

[37] M. Sadeghi-Aghbash, M. Rahimnejad, H. Adeli, F. Feizi, Fabrication and development of PVA/Alginate nanofibrous mats containing Arnebia Euchroma extract as a burn wound dressing, React. Funct. Polym. 181 (2022) 105440, https://doi.org/10.1016/j.reactfunctpolym.2022.105440.

[38] Y.R. Corrales-Ureña, Z. Souza-Schiaber, P.N. Lisboa-Filho, F. Marquenet, P.-L. Michael Noeske, L. Gätjen, K. Rischka, Functionalization of hydrophobic surfaces with antimicrobial peptides immobilized on a bio-interfactant layer, RSC Adv. 10 (2020) 376–386, https://doi.org/10.1039/C9RA07380A.

[39] M.T.H. Nguyen, D. Biriukov, C. Tempra, K. Baxova, H. Martinez-Seara, H. Evci, V. Singh, R. Šachl, M. Hof, P. Jungwirth, M. Javanainen, M. Vazdar, Ionic Strength and Solution Composition Dictate the Adsorption of Cell-Penetrating Peptides onto Phosphatidylcholine Membranes, Langmuir 38 (2022) 11284–11295, https://doi.org/10.1021/acs.langmuir.2c01435.

[40] H. Chen, X. Su, K.-G. Neoh, W.-S. Choe, Context-Dependent Adsorption Behavior of Cyclic and Linear Peptides on Metal Oxide Surfaces, Langmuir 25 (2009) 1588–1593, https://doi.org/10.1021/la8030304.

[41] W.-S. Choe, M.S.R. Sastry, C.K. Thai, H. Dai, D.T. Schwartz, F. Baneyx, Conformational Control of Inorganic Adhesion in a Designer Protein Engineered for Cuprous Oxide Binding, Langmuir 23 (2007) 11347–11350, https://doi.org/10.1021/la702414m.

[42] I.E. Ivanov, A.E. Morrison, J.E. Cobb, C.A. Fahey, T.A. Camesano, Creating Antibacterial Surfaces with the Peptide Chrysophsin-1, ACS Appl. Mater. Interfaces 4 (2012) 5891–5897, https://doi.org/10.1021/am301530a.

[43] J.S. Evans, Tuning in" to Mollusk Shell Nacre- and Prismatic-Associated Protein Terminal Sequences. Implications for Biomineralization and the Construction of High Performance Inorganic−Organic Composites, Chem. Rev. 108 (2008) 4455–4462, https://doi.org/10.1021/cr078251e.

[44] S.-H. Joo, Cyclic Peptides as Therapeutic Agents and Biochemical Tools, Biomol. Ther. (Seoul.) 20 (2012) 19–26, https://doi.org/10.4062/biomolther.2012.20.1.019.

[45] A. Bin Hafeez, X. Jiang, P.J. Bergen, Y. Zhu, Antimicrobial Peptides: An Update on Classifications and Databases, Int J. Mol. Sci. 22 (2021) 11691, https://doi.org/10.3390/ijms222111691.

[46] M. Coste, E. Suárez-Picado, S. Ulrich, Hierarchical self-assembly of aromatic peptide conjugates into supramolecular polymers: it takes two to tango, Chem. Sci. 13 (2022) 909–933, https://doi.org/10.1039/D1SC05589E.

[47] J. Liu, M.L. Lee, Permanent surface modification of polymeric capillary electrophoresis microchips for protein and peptide analysis, Electrophoresis 27 (2006) 3533–3546, https://doi.org/10.1002/elps.200600082.

[48] A. Vedadghavami, C. Zhang, A.G. Bajpayee, Overcoming negatively charged tissue barriers: Drug delivery using cationic peptides and proteins, Nano Today 34 (2020) 100898, https://doi.org/10.1016/j.nantod.2020.100898.

[49] X. Wu, P. Wei, X. Zhu, M.J. Wirth, A. Bhunia, G. Narsimhan, Effect of immobilization on the antimicrobial activity of a cysteine-terminated antimicrobial Peptide Cecropin P1 tethered to silica nanoparticle against E. coli O157: H7 EDL933, Colloids Surf. B Biointerfaces 156 (2017) 305–312, https://doi.org/10.1016/j.colsurfb.2017.05.047.

[50] M. Wiśniewska, V. Bogatyrov, I. Ostolska, K. Szewczuk-Karpisz, K. Terpiłowski, A. Nosal-Wiercińska, Impact of poly(vinyl alcohol) adsorption on the surface characteristics of mixed oxide Mn x O y –SiO2, Adsorption 22 (2016) 417–423, https://doi.org/10.1007/s10450-015-9696-2.

[51] S. Swiatek, P. Komorek, B. Jachimska, Adsorption of β-lactoglobulin A on gold surface determined in situ by QCM-D measurements, Food Hydrocoll. 91 (2019) 48–56, https://doi.org/10.1016/j.foodhyd.2019.01.007.

[52] R. Hajiraissi, M. Hanke, Y. Yang, B. Duderija, A. Gonzalez Orive, G. Grundmeier, A. Keller, Adsorption and fibrillization of islet amyloid polypeptide at self-assembled monolayers studied by QCM-D, AFM, and PM-IRRAS, Langmuir 34 (2018) 3517–3524, https://doi.org/10.1021/acs.langmuir.7b03626.

[53] K. Lyu, H. Chen, J. Gao, J. Jin, H. Shi, D.K. Schwartz, D. Wang, Protein desorption kinetics depends on the timescale of observation, Biomacromolecules 23 (2022) 4709–4717, https://doi.org/10.1021/acs.biomac.2c00917.